J. Fluid Mech. (2020), *vol.* 886, A30. © The Author(s), 2020.
Published by Cambridge University Press
doi:10.1017/jfm.2019.1072

Spin coating of capillary tubes

B. K. Primkulov[1], A. A. Pahlavan[2], L. Bourouiba[1], J. W. M. Bush[3] and R. Juanes[1,†]

[1]Department of Civil and Environmental Engineering, Massachusetts Institute of Technology, 77 Massachusetts Avenue, Cambridge MA 02139, USA

[2]Mechanical and Aerospace Engineering Department, Princeton University, Olden St., Princeton NJ 08544, USA

[3]Department of Mathematics, Massachusetts Institute of Technology, 77 Massachusetts Avenue, Cambridge MA 02139, USA

(Received 25 May 2019; revised 18 December 2019; accepted 19 December 2019)

We present the results of a combined experimental and theoretical study of the spin coating of the inner surface of capillary tubes with viscous liquids, and the modified Rayleigh–Plateau instability that arises when the spinning stops. We show that during the spin coating, the thinning of the film is governed by the balance of viscous and centrifugal forces, resulting in the film thickness scaling as $h \sim t^{-1/2}$. We demonstrate that the method enables us to reach uniform micrometre-scale films on the tube walls. Finally, we discuss potential applications with curable polymers that enable precise control of film geometry and wettability.

Key words: thin films, coating

1. Introduction

Use of capillary tubes is widespread in a range of health and industrial applications, for example, in the studies of film instability (Goren 1962; Rossen 2000; Duclaux, Clanet & Quéré 2006), wetting (Washburn 1921; Hoffman 1975; Walls, Dequidt & Bird 2016; Zhao *et al.* 2018), blood flow (Goldsmith & Spain 1984; Pries, Neuhaus & Gaehtgens 1992) and oil recovery (Blunt 2001; Morrow & Mason 2001; Patzek & Kristensen 2001). In many of these applications, precise control of the surface properties of the capillary tubes is critical. Here, we demonstrate that such control is possible through the deposition of thin layers of functional polymers via spin coating (Emslie, Bonner & Peck 1958; Scriven 1988), a technique that has not previously been explored for coating capillary tubes.

The prevalent approach to coating the inner wall of a capillary tube dates back to Taylor (1961). A tube is filled with viscous liquid, which is subsequently expelled by air at a prescribed flow rate. As the air bubble propagates through the tube, a liquid film of uniform thickness is left on the wall of the tube. When $Ca \ll 1$, the thickness h can be estimated from Bretherton's law (Bretherton 1961) as $h \sim RCa^{2/3}$, where $Ca = \mu u/\sigma$ is the capillary number, μ the liquid viscosity, u the bubble velocity, σ

† Email address for correspondence: juanes@mit.edu

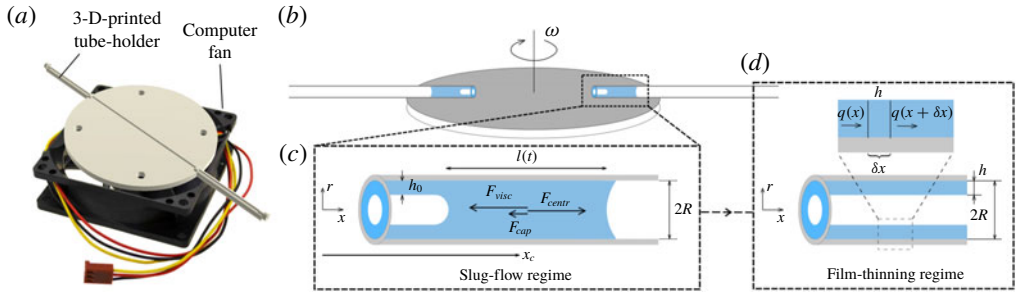

FIGURE 1. (*a*) Diagram of the computer fan repurposed as a spin coater. (*b*) Schematic of the capillary tubes filled with liquid slugs, spun at angular velocity ω. (*c*) Schematic of the slug-flow regime. (*d*) Schematic of the film-thinning regime. 3-D, three-dimensional.

the surface tension and R the tube radius. This method has been used extensively to generate annular films of controlled thickness (Goren 1962; Aussillous & Quéré 2000; Duclaux *et al.* 2006). While it is well suited to generating relatively thick films at moderate bubble speeds, practical difficulties in maintaining very low gas flow rates may preclude the deposition of films of uniform thickness at very low displacement rates. In particular, syringe pumps operating at low constant injection rates are known to have stepper-motor-induced pressure fluctuations (Li *et al.* 2014; Zeng *et al.* 2015).

Here, we explore centrifugally forced deposition of viscous liquids in capillary tubes, which offers an easily accessible alternative to Taylor's method that is particularly advantageous for micron-scale films. In § 2, we describe the details of the experimental set-up. We present theoretical arguments for the early and late-time flow dynamics in § 3. Control over the film thickness allows for manipulation of the time scale of the subsequent Rayleigh–Plateau instability described in § 5. We thus present methods for generating both cylindrical and corrugated coatings on capillary tubes with a curable polymer, and point to potential applications in § 6.

2. Experimental method

We repurpose a computer fan as a spin coater: the blades of the fan are removed and a three-dimensionally printed platform for holding capillary tubes is attached, centred at the spin axis (figure 1*a*). The fan is connected through an Arduino board to MATLAB, where we fix the angular velocity at 854 ± 10 r.p.m. for all of the experiments presented below.

First, we explore how liquid slugs move within the spinning capillary tubes with high speed imaging (see the supplementary material, available at https://doi.org/10.1017/jfm.2019.1072, Movie 1). We introduce 20 mm long liquid slugs into the capillary tubes (Hilgenberg borosilicate glass, 75 mm in length, 290 μm inner radius), place them onto the spin-coating platform, as shown in figure 1(*b*), and spin. We track the slug length $l(t)$ and slug-centre distance $x_c(t)$ from the spin axis (figure 2*a*,*b*). As the slug moves outwards, it leaves a film of liquid behind, reducing the slug length l as x_c increases. Notably, the evolution of l with x_c is nearly independent of the liquid viscosity (figure 2*b*), which means that the film thickness profile deposited by the slug is also independent of viscosity. Furthermore, x_c grows exponentially with time (figure 2*a*), which makes the slug-flow regime very brief. Both of these observations are to be rationalized in § 3.2.

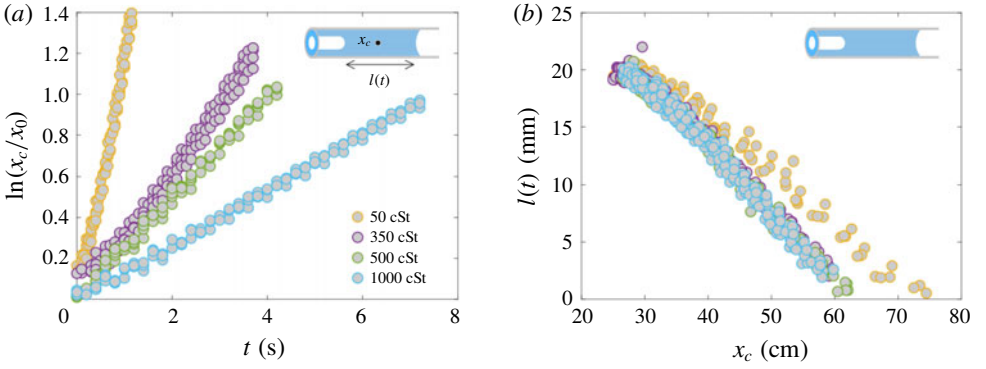

FIGURE 2. (*a*) Exponential change in the slug-centre position x_c with time, where the time scales (inverse of the slope) are [0.9, 3.2, 4.0, 7.5] s for [50, 350, 500, 1000] cSt, respectively. Here x_0 is the initial coordinate of the slug centre. (*b*) Measurements of the slug length l with x_c suggest viscosity-independent film-deposition profiles (see appendix A for a discussion of the deviation of the 50 cSt oil curve).

In the second set of experiments, we explore the thinning dynamics of the liquid films on the capillary tube walls arising after the slug has exited the tube. We introduce a sufficient volume of liquid into the capillary tubes such that the film is deposited throughout the tube. The excess liquid is allowed to escape from the outer end of the tube. The thickness of the liquid film left on the walls is estimated from the weight difference of the dry and coated tubes. This is done in groups of ten capillary tubes – weights are measured with an Ohaus Explorer EX225D scale, which allows 0.1 mg precision, corresponding to sub-micrometre precision in the final film thickness.

When capillary tubes are spun at sufficiently high angular speed, the amount of liquid within the tubes drops sharply at first, then slowly approaches its long-time limit. The experimental results of spin-coating capillary tubes with different liquids (50–1000 cSt silicone oils and NOA81) are reported in figure 3(*a*). Silicone oils and NOA81 show similar trends, with the value of the final thickness increasing with viscosity.

We rationalize these observations with theoretical models developed in the next section, where we distinguish two flow modes: slug motion and film thinning. We find the characteristic time scales of these two modes and show that the temporal evolution evident in figure 3 is largely associated with the slow thinning of the viscous films. Note that we do not attempt to model the film thinning of NOA81, as its rheology is yet to be fully characterized. We found that its viscosity (∼240 cSt) increases with shelf life and that it exhibits non-Newtonian behaviour at low film heights. As a result, the polymer is primarily used here to illustrate the possibility of making channels with wavy walls in § 6.

3. Theory

Consider a capillary tube, containing a liquid slug of density ρ and dynamic viscosity μ, that is spun at a prescribed angular speed ω (figure 1*c*). As the slug moves outwards, it deposits a liquid film on the tube walls. We consider the control region containing the slug only. Three forces may be significant in this configuration:

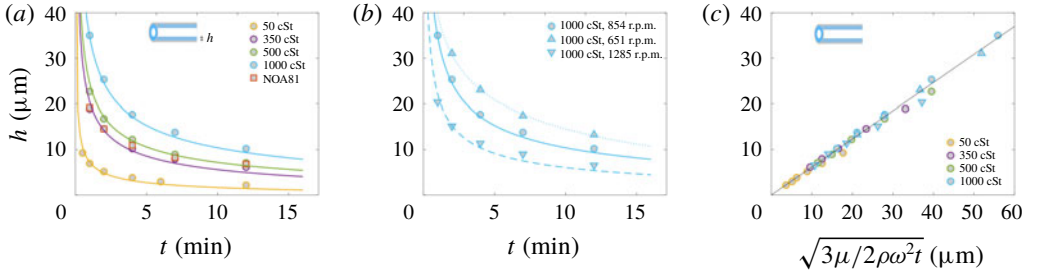

FIGURE 3. (*a*) Temporal evolution of the deposited film thickness long after the slug motion: measurements are denoted with circles (and squares), theory with solid lines. (*b*) Film thickness evolution of 1000 cSt silicone oil spun at 651, 854 and 1285 r.p.m. (*c*) Collapse of the data from figure 3(*a*) and figure 3(*b*) using (3.11). Each point corresponds to 10 spin-coating experiments, with over 350 total coated tubes.

the capillary (F_{cap}), viscous (F_{visc}) and centrifugal (F_{centr}) forces. The capillary force can be estimated from the different end curvatures of the liquid slug; the Laplace pressure difference on its ends opposes the outward motion (Bico & Quéré 2001):

$$F_{cap} = -\pi R^2 \frac{2\sigma}{R} + \pi (R - h_0)^2 \frac{2\sigma}{R - h_0} = -2\pi\sigma h_0,$$

where h_0 is the characteristic thickness of the film deposited by the slug motion, and we assume a completely wetting liquid. The viscous force associated with Poiseuille flow can be estimated from the drag on the tube walls,

$$F_{visc} = -2\pi R l(t) \frac{4\mu}{R} \dot{x}_c = -8\pi\mu l(t) \dot{x}_c,$$

where $l(t)$ is the liquid slug length, x_c the position of the slug centre and $\dot{x}_c$ its velocity. Finally, the centrifugal force acting at the slug can be expressed as

$$F_{centr} = \int_{x_c - l/2}^{x_c + l/2} \rho \pi R^2 \omega^2 x \, \mathrm{d}x = \rho \pi R^2 \omega^2 l(t) x_c.$$

Therefore, the motion of the slug is governed by $\mathrm{d}(m\dot{x}_c)/\mathrm{d}t = F_{cap} + F_{visc} + F_{centr}$, from which it follows that

$$\frac{\dot{m}\dot{x}_c}{m} + \ddot{x}_c = -\frac{2\sigma h_0}{\rho l(t) R^2} - \frac{8\mu \dot{x}_c}{\rho R^2} + \omega^2 x_c.$$

We neglect $\dot{m}\dot{x}_c$ since $\dot{m}\dot{x}_c/m\ddot{x}_c = \rho 2\pi R h_i \dot{x}_c^2 / \rho \pi R^2 l \ddot{x}_c = (h_i/R)(2\dot{x}_c^2/\ddot{x}_c l) \sim (h_i/R)(l^2/\tau_{inert}^2 / l^2/\tau_{inert}^2) = h_i/R \ll 1$, where h_i is the film thickness deposited in the inertial regime and τ_{inert} the inertial time scale (see § 3.1). Furthermore, $F_{cap}/F_{centr} = (h/R)(2\sigma/\rho l x_c R\omega^2) \sim 10^{-2}(h/R) \ll 1$; hence, we may safely neglect the contribution of the capillary force from this point on. The force balance then reduces to

$$\ddot{x}_c = -\frac{8\mu \dot{x}_c}{\rho R^2} + \omega^2 x_c. \tag{3.1}$$

We proceed by separating the slug dynamics (figure 1*c*) into early inertial (§ 3.1) and late viscous (§ 3.2) regimes. The subsequent thinning of the film on the tube walls (figure 1*d*) is described thereafter.

3.1. *Inertial slug flow* ($t < \rho R^2/8\mu$)

When the flow is dominated by inertia, the viscous term in (3.1) can be neglected and the motion of the slug is governed by

$$\ddot{x}_c = \omega^2 x_c. \tag{3.2}$$

The position of the slug can be expressed as $x_c(t) = x_0 \cosh(\omega t)$, where x_0 is the initial coordinate of the slug centre.

The inertial flow persists until the boundary effects diffuse across the tube and motion becomes viscosity dominated. The cross-over between the two regimes occurs when the viscous term becomes comparable to inertia and $\ddot{x}_c \sim 8\mu\dot{x}_c/\rho R^2$, which allows us to establish the characteristic time for the inertial flow as $\tau_{inert} \equiv \rho R^2/8\mu$. The characteristic time scale of inertial slug flow ranges between 10^{-5} and 2×10^{-4} s for the silicone oils used in our study. Notably, these times correspond to the oil slug displacements between 8 nm and 3 μm (for 1000 cSt and 50 cSt oils, respectively): in our experiments, the system quickly switches to the viscosity-dominated regime.

3.2. *Viscous slug flow* ($\rho R^2/8\mu < t < 8\mu/\rho\omega^2 R^2$)

In the viscosity-dominated slug regime, we neglect the inertial terms so that (3.1) reduces to

$$\frac{8\mu\dot{x}_c}{\rho R^2} = \omega^2 x_c, \tag{3.3}$$

and the slug position can be expressed as $x_c = x_0 \mathrm{e}^{(\rho\omega^2 R^2/8\mu)t}$. The characteristic time for the slug flow is $\tau_{slug} \equiv 8\mu/\rho\omega^2 R^2$, which corresponds to 0.6 and 11.7 s for 50 and 1000 cSt silicone oils, respectively. These times are in close agreement with the experimental measurements of the slug-flow time scale reported in figure 2(*a*).

As the liquid slug moves through the tube, it deposits a film on the wall. This film is also subject to centrifugal forces; however, we neglect its thinning within the relatively brief time frame of the viscous slug flow (an approximation to be justified *a posteriori* by comparison with the thinning time scale). Then, the thickness of the deposited film can be estimated from Bretherton's scaling (Bretherton 1961) as

$$h_0(x) \sim RCa^{2/3} = R\left(\frac{\mu\dot{x}}{\sigma}\right)^{2/3} = R\left(\frac{\rho\omega^2 R^2}{8\sigma}x\right)^{2/3}. \tag{3.4}$$

Notably, this thickness is independent of the liquid viscosity, in agreement with the experimental data in figure 2(*b*).

As the slug speed increases, the Ca increases from 0 to approximately 0.8 in our experiments. Therefore, Bretherton's scaling (3.4) is only applicable while the slug is near the inner end of the tube, where $Ca \ll 1$. While a more accurate scaling of $h_o(x) \sim R(Ca^{2/3}/(1 + Ca^{2/3}))$ can be used for Ca between 0.01 and 1 (Aussillous & Quéré 2000), we demonstrate in § 4 that the late-time thinning profile is not sensitive to the film thickness profile left after the viscous slug-flow regime. This is consistent with the work of Emslie *et al.* (1958). Therefore, we use the expression (3.4) as a leading-order approximation for simplicity in this work.

3.3. *Film thinning* ($t > 8\mu/\rho\omega^2R^2$)

In the late-time flow regime, we start with the film thickness profiles from (3.4). Subsequent thinning of the film is resisted predominantly by the viscosity of the liquid. As the liquid film thins, viscous resistance balances the centrifugal force, $F_{visc} \sim F_{centr}$, as is the case in the spin coating of flat surfaces (Emslie *et al.* 1958). Then, in the absence of inertia and provided that $h \ll R$, we can invoke the lubrication approximation, according to which

$$0 = \mu \frac{\partial^2 u}{\partial r^2} + \rho\omega^2 x. \tag{3.5}$$

By imposing the no-slip boundary condition at the wall and zero shear stress at the liquid surface, we obtain from direct integration of (3.5) the velocity field: $u(x, r) = (\rho\omega^2 x/\mu)(-r^2/2 + r(R - h(x)) + R(h(x) - R/2))$. Thus, we estimate the volume flow rate as

$$q(x) = \int_{R-h(x)}^{R} 2\pi r u(x, r)\, \mathrm{d}r = \frac{\pi\rho h(x)^3\omega^2 x}{12\mu}(8R - 5h(x)). \tag{3.6}$$

Conservation of mass in a representative section of the liquid film (see figure 1*d*) yields $q(x) - q(x + \delta x) = 2\pi(R - h(x))\delta h\delta x/\delta t$, which can be rewritten as

$$\frac{\mathrm{d}h}{\mathrm{d}t} = -\frac{1}{2\pi(R - h(x))}\frac{\mathrm{d}q(x)}{\mathrm{d}x}. \tag{3.7}$$

This is a first-order partial differential equation for $h(t, x)$, equivalent to

$$\frac{24\mu(R - h)}{\rho\omega^2}\frac{\mathrm{d}h}{\mathrm{d}t} + 4xh^2(6R - 5h)\frac{\mathrm{d}h}{\mathrm{d}x} = -h^3(8R - 5h). \tag{3.8}$$

If we define $\mathrm{d}n \equiv \rho\omega^2\mathrm{d}t/24\mu(R - h) = \mathrm{d}x/4xh^2(6R - 5h) = -\mathrm{d}h/h^3(8R - 5h)$, then the solution of (3.8) can be written as (Cheng 2007)

$$\frac{\mathrm{d}t}{\mathrm{d}n} = \frac{24\mu(R - h)}{\rho\omega^2}, \quad \frac{\mathrm{d}x}{\mathrm{d}n} = 4xh^2(6R - 5h), \quad \frac{\mathrm{d}h}{\mathrm{d}n} = -h^3(8R - 5h). \tag{3.9a–c}$$

Evolution of the film thickness can be resolved by taking the (x, h) coordinates of Bretherton's film from (3.4), and solving the system (3.9). We do so for all silicone oils used in our experiments and plot the theoretical film thicknesses in figure 3(*a*) and figure 3(*b*), where the theory closely matches the experimental measurements. The typical temporal evolution of the liquid thickness profiles is reported in figure 4(*a*). Noting that the scales of the vertical and horizontal axes are very different in figure 4(*a*), we see that when capillary tubes are spun at high ω, the film thickness very quickly becomes nearly uniform. In that case, $\mathrm{d}h/\mathrm{d}x \ll 1$ and (3.7) yields $\mathrm{d}h/\mathrm{d}t = -(\rho\omega^2h^3/24\mu)((8R - 5h)/(R - h))[1 + (3x/h)(1 - (5/24)(h/R))(\mathrm{d}h/\mathrm{d}x)]$ which reduces to

$$\frac{\mathrm{d}h}{\mathrm{d}t} = -\frac{\rho\omega^2h^3}{24\mu}\frac{8R - 5h}{R - h}. \tag{3.10}$$

We note that in the above approximation, the rate of thinning is independent of x. This feature is consistent with numerous spin-coating applications in which the film thickness is known to be nearly uniform and insensitive to the initial shape of the liquid bulk (Emslie *et al.* 1958; Scriven 1988).

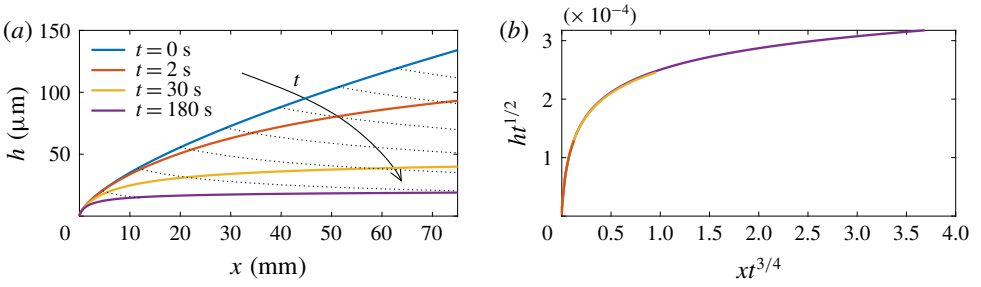

FIGURE 4. (*a*) Silicone oil (500 cSt) film thickness profiles at various times, where the initial profile (blue) is estimated with (3.4). Subsequent thickness profiles are obtained by evolving the surface coordinates with the system (3.9). Dotted lines represent the material point trajectories. (*b*) Collapse of the film thinning profiles onto a single curve via the similarity transformation developed in § 4.

Since $h \ll R$, the expression (3.10) reduces to $\mathrm{d}h/\mathrm{d}t = -\rho\omega^2 h^3/3\mu$. Then, the evolution of the film thickness is independent of the tube radius, and integration yields

$$h_0^{-2} - h^{-2} = -\frac{2\rho\omega^2}{3\mu}t. \tag{3.11}$$

This suggests that if we plot the data in figure 2(*a*,*b*) as h against $\sqrt{3\mu/2\rho\omega^2 t}$, when $h \ll h_0$ the data should collapse onto a straight line, as is indeed evident in figure 3(*c*). The characteristic time scale of the film thinning changes with the film thickness as $\tau_{thinning} \equiv 3\mu/2\rho\omega^2 h^2$, which is significantly larger than the time scale of the viscous slug motion: $\tau_{slug}/\tau_{thinning} = h^2/R^2 \ll 1$. This disparity in the time scales justifies our neglecting the film thinning in § 3.2.

4. Self-similar solution of film thinning

We proceed by developing a similarity solution suggested by our governing equations. The film thinning in capillary tubes is governed by (3.8), which can be rewritten as

$$k_2(R-h)\frac{\mathrm{d}h}{\mathrm{d}t} + 4xh^2(6R-5h)\frac{\mathrm{d}h}{\mathrm{d}x} = -h^3(8R-5h), \tag{4.1}$$

where $k_2 = 24\mu/\rho\omega^2$. The initial conditions are set by

$$h(0, x) = k_1 x^{2/3}, \tag{4.2}$$

where $k_1 = R(\rho\omega^2 R^2/8\sigma)^{2/3}$.

The equations of characteristics for (4.1) yield (Cheng 2007):

$$\frac{\mathrm{d}t}{k_2(R-h)} = \frac{\mathrm{d}x}{4xh^2(6R-5h)} = -\frac{\mathrm{d}h}{h^3(8R-5h)}. \tag{4.3}$$

Resolving the first and second equalities in (4.3) results in the following equations:

$$\ln x = \frac{4h^2(6R-5h)}{k_2(R-h)}t + \ln c_1 \quad \text{and} \quad \ln x = -3\ln h - \ln(h-8R/5) + \ln c_2,$$

which simplify to

$$x = c_1 \mathrm{e}^{(4h^2(6R-5h)/k_2(R-h))t} \quad \text{and} \quad x = \frac{c_2}{h^3(h-8R/5)},$$

respectively, with

$$c_1 = x\mathrm{e}^{-(4h^2(6R-5h)/k_2(R-h))t} \equiv f(t, x, h) \quad \text{and} \quad c_2 = xh^3(h-8R/5) \equiv g(t, x, h). \quad (4.4a,b)$$

With given values of c_1 and c_2, equation (4.4) describes two-dimensional surfaces in (t, x, h) space. The intersection of these two surfaces is a characteristic curve, and one obtains the characteristic curves of (4.1) by spanning all possible combinations of c_1 and c_2. The solution that satisfies the initial condition (4.2) can be found graphically (Cheng 2007). We choose characteristic curves that pass through points $(0, x, h(0, x))$, and the aggregate of these curves forms a solution surface in the (t, x, h) space.

Alternatively, one can find the analytical solution by finding the curves that satisfy the relation

$$c_1 = F(c_2) \quad \text{or} \quad g(t, x, h) = F(f(t, x, h)), \quad (4.5a,b)$$

where F is an arbitrary function. Here, equation (4.5) is the general solution of (4.1), and the function F can be determined from the initial condition $g(0, x, h(0, x)) = F(f(0, x, h(0, x)))$, which using $h(0, x)$ from (4.2) yields

$$F(x) = k_1^3 x^3 (k_1 x^{2/3} - 8R/5). \quad (4.6)$$

Finally, the general solution of (4.1) with initial condition (4.2) is $g(t, x, h) = F(f(t, x, h))$, which can be rewritten as $g = k_1^3 f^3 (k_1 f^{2/3} - 8R/5)$ or

$$xh^3(h-8R/5) = k_1^3[x\mathrm{e}^{-(4h^2(6R-5h)/k_2(R-h))t}]^3(k_1[x\mathrm{e}^{-(4h^2(6R-5h)/k_2(R-h))t}]^{2/3} - 8R/5). \quad (4.7)$$

Here, (4.7) can be solved implicitly for h given a combination of t and x. When solved for 500 cSt silicone oil spun at 854 r.p.m., (4.7) produces the curves in figure 4(*a*).

The solution (4.7) at later times, when $h \ll R$ and $t \gg 1$, reduces to

$$xh^3 = k_1^3 x^3 \mathrm{e}^{-(24h^2/k_2)t}. \quad (4.8)$$

We substitute $h = t^\alpha H$ and $x = t^\beta \xi$ into (4.8) to obtain

$$t^{3\alpha-2\beta}\frac{H^3}{\xi^2} = k_1^3 \mathrm{e}^{-(24H^2/k_2)t^{2\alpha+1}}. \quad (4.9)$$

The profile $H(\xi)$ is self-similar when (4.9) is independent of t. This happens when

$$3\alpha - 2\beta = 0 \quad \text{and} \quad 2\alpha + 1 = 0, \quad \text{or equivalently} \quad \alpha = -1/2, \ \beta = -3/4.$$

Plotting $ht^{1/2}$ versus $xt^{3/4}$ collapses all curves from figure 4(*a*) onto the self-similar profile shown in figure 4(*b*).

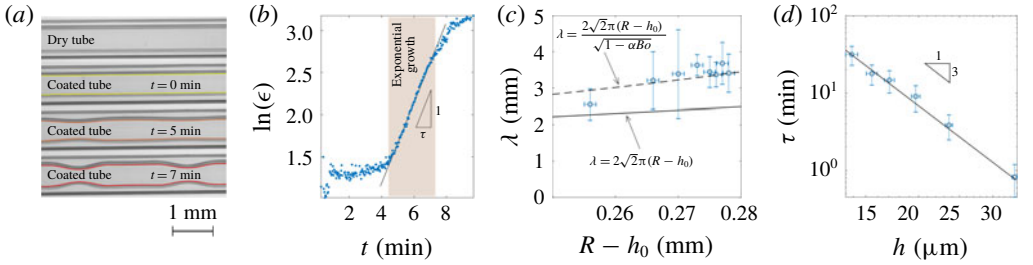

FIGURE 5. Rayleigh–Plateau instability of 500 cSt silicone oil films. (*a*) Typical temporal evolution of liquid film instability. Note that the liquid–solid boundary is not visible because the refractive indices of the oil ($n = 1.41$) and glass ($n = 1.51$) are very similar. (*b*) Evolution of the Rayleigh–Plateau crest thickness ϵ. The instability time scale τ is the inverse of the slope. Such plots are used to measure τ values in figure 5(*d*). (*c*) Measurements of instability wavelengths. (*d*) The time scale of the Rayleigh–Plateau instability, as estimated from the slope of the linear portion of $\ln(\epsilon(t))$ in figure 5(*b*). The film thickness is estimated from (3.10). A conservative estimate of the error is taken as the largest difference between the experimental and theoretical film thicknesses in figure 3(*a*). Vertical error bars represent standard deviations in both (*c*) and (*d*).

5. Rayleigh–Plateau instability

Having produced nearly uniform micrometre-scale films on the inner walls of the capillary tubes by spin coating over the time scales reported in figure 3(*a*), we stop the spinning, making F_{centr} vanish. In this setting, the ratio of gravitational to capillary forces is relatively low, so that $Bo \equiv (R - h_0)^2/\ell_{cap}^2 \approx 0.04$, where $\ell_{cap} \equiv \sqrt{\sigma/\rho g}$ is the capillary length. Therefore, these thin films are subject to Rayleigh–Plateau instability (figure 5*a*), with the fastest growing wavelength and time scale of the instability depending on the film thickness h_0 after spin coating (Goren 1962; Duclaux *et al.* 2006; Eggers & Villermaux 2008). Consequently, one should be able to control these parameters by tuning the spinning and curing times of the polymer film, thereby generating either flat or wavy surfaces inside the capillary tubes.

We track the temporal progression of the film instability by detecting inner boundaries of the liquid from the top-view images of the experiment (figure 5*a*). The wavelength of instability λ is measured as the distance between the crests on the liquid surface. Depending on h_0, the mean experimental values of λ range between 2.5 and 3.5 mm (figure 5*c*), which are approximately 32 % higher than the expected wavelength of $\lambda \sim 2\sqrt{2}\pi(R - h_0)$ for viscous annular films (Goren 1962). This discrepancy has been attributed to gravity effects by Duclaux *et al.* (2006), who suggested a corrected expression for the wavelength of $\lambda \sim 2\sqrt{2}\pi(R - h_0)/\sqrt{1 - \alpha Bo}$, where α is an empirical coefficient. Adapting this expression would require $\alpha \approx 12$ to fit our data. Duclaux *et al.* (2006) outline three distinct regimes of film instability in terms of two parameters: $\sqrt{Bo}$ and $Bo(R - h_0)/h_0$. When $\sqrt{Bo} \ll 1$ and $Bo(R - h_0)/h_0 \ll 1$, the effects of gravity are negligible and the classical wavelength of $\lambda \sim 2\sqrt{2}\pi(R - h_0)$ is recovered (Goren 1962). When $\sqrt{Bo} \ll 1$ and $Bo(R - h_0)/h_0 = O(1)$, the wavelength is unaffected, but the instability grows faster on the lower side of the horizontal tube. Finally, as $\sqrt{Bo}$ approaches $O(1)$, the wavelength increases as compared to the classical scaling. In our experiments $\sqrt{Bo} \approx 0.2$, hence the wavelength λ is quite possibly being affected by gravitational effects.

Despite the discrepancy in the observed wavelength, our measurements of the instability time scale closely match the theory. The growth rate is expected to follow an exponential law $\mathrm{d}\epsilon/\mathrm{d}t \sim \tau^{-1}\epsilon$, where τ is the characteristic time scale (Plateau 1873; Rayleigh 1892). Indeed, significant portions of the $h(t)$ are linear on a semi-logarithmic plot (figure 5*b*). The time scales τ for different h_0 are estimated from the slopes of these linear sections. The experimental data follow the theoretically expected scaling of $\tau \sim \mu(R-h_0)^4/\sigma h_0^3$ (Goren 1962; Johnson *et al.* 1991), which reduces to $\tau \sim \mu R^4/\sigma h_0^3$ for thin films (see figure 5*d*).

We observe that Rayleigh–Plateau instabilities grow nearly simultaneously throughout the capillary tubes in all of our experiments (see supplementary material, Movie 2). Therefore, the data in figure 5(*d*) provide further confirmation that centrifugal spin coating produces films of nearly uniform thickness on the tube wall. Note that as the film thickness changes from 20 to 13 μm, the characteristic time scale of instability changes from a minute to more than an hour (figure 5*d*). If the film thickness were to change appreciably from one end of the tube to the other, we would thus expect to see significant variations in the time scale of the Rayleigh–Plateau instability along the tube, which is not the case in our experiments.

6. Coating with curable polymers

Having explored the coating of the capillary tubes with 500 cSt silicone oil and the subsequent instability of the resulting films, we illustrate one particularly interesting application of the spin-coating method. We coat the inner walls of two capillary tubes with a 13 μm film of NOA81. We cure one tube with UV light immediately after depositing the film, and let the other form Rayleigh–Plateau instabilities for one hour prior to curing. By doing so, we fabricate two capillary tubes: one with straight and the other with wavy inner walls. Since these surfaces are generated by curing liquid polymers, one may obtain surfaces that are smooth down to a molecular scale (de Gennes, Brochard-Wyart & Quéré 2004).

Capillary tubes are often used in flow experiments as analogues of porous media. The two tubes we generated here represent two types of pore channels. Liquid should spontaneously imbibe into them following the Washburn law (Washburn 1921) $L \sim ((R-h_0)\sigma/2\mu t)^{1/2}$, where L is the axial distance of the liquid penetration. Since both tubes have nearly identical mean inner radii, we expect that their experimental $L(t)$ curves would be nearly identical, with both following $L(t) \sim t^{1/2}$. This is indeed the case (figure 6), with an important distinction between the two: the liquid in a wavy tube gets intermittent boosts in the capillary driving force whenever the liquid front passes through constrictions in the film's wavy pattern. This effect results in a distinct temporal profile of the liquid in a wavy tube compared to that in a flat one (figure 6).

7. Conclusion

We have proposed and realized experimentally a robust and practical method of spin coating the inner wall of capillary tubes with viscous liquids. We first demonstrated the dynamics of centrifugally driven slug motion within the tubes. We then showed that the dynamics of the film thinning is governed by the balance of viscous and centrifugal forces, and that the thickness of the film can be anticipated through theoretical arguments. The method of coating presented here is an alternative to that of Taylor (1961), and is well suited to generating micron-scale liquid films.

The ability to produce both cylindrical and undulatory inner surfaces may be useful in many practical applications. For instance, coating capillary tubes with

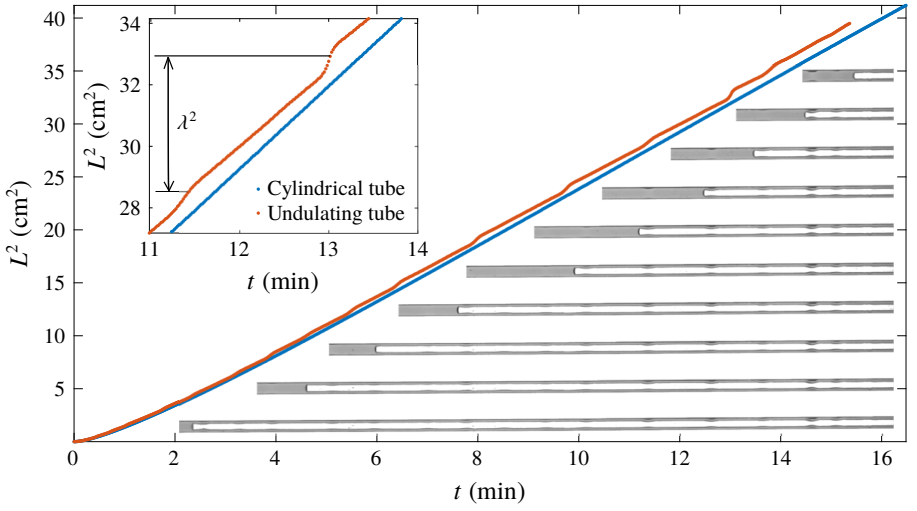

FIGURE 6. Capillary imbibition of silicone oil in two horizontal capillary tubes coated with NOA81: one with a flat, another with a corrugated inner channel. The inset shows the temporary acceleration of the liquid interface arising at the narrowest parts of the channel.

NOA81 would allow for careful control of the substrate wettability (Zhao, MacMinn & Juanes 2016; Odier *et al.* 2017), while having wavy inner surfaces may prove useful in studying the pinch-off and trapping of the resident liquid in porous media. Finally, the inner wall of the tubes can be coated sequentially with polymers with different electric conductivity, which would allow for the generation of electrowetting (Mugele & Baret 2005), where wettability may be modulated by a time-varying electric current. This may ultimately enable the manufacturing of capillary tubes that act like pressure oscillators in microfluidic devices.

Acknowledgements

We thank J. Chui and E. Haghighat for helpful discussions, S. Rudolph for technical support, J. W. Bales from the Edgerton Centre at MIT for the imaging support and insights and R. Dandekar for help with the portion of the rheology measurements. This work was funded by the KFUPM-MIT collaborative agreement 'Multiscale Reservoir Science'.

Declaration of interests

The authors report no conflict of interest.

Supplementary movies

Supplementary movies are available at https://doi.org/10.1017/jfm.2019.1072.

Appendix A. Spin-coater speed and experimental data

In this section we assess two potential sources of error that come from the design of the spin-coater system. First, it takes approximately 1 s for our computer fan to reach its target speed. Second, the speed of the computer fan is found to fluctuate within

a ± 10 r.p.m. window, which has implications for the error in the film thickness. The size of the error window would depend on the details of the electric circuit and power source. We took steps to reduce the heating of the electric components and variations in the power supply from the building in order to minimize the error.

A.1. *Deviation of 50 cSt oil from more viscous oils in figure 2(b)*

The discrepancy between the 50 cSt silicone oil and more viscous oils stems from the fact that it takes ~ 1 s for the fan to reach the target speed of 854 r.p.m. Incidentally, the characteristic time scale for the slug flow of 50 cSt silicone oil is 0.9 s (figure 2*a*). As a result, the 50 cSt silicone oil slug-flow regime effectively sets in at lower angular velocity, 673 r.p.m. compared to 854 r.p.m. for higher viscosity oils. This results in a thinner initial film coating, which explains the deviation in the $l(x_c)$ profile evident in figure 2(*b*).

A.2. *Estimating film thickness variation in comparison to Taylor's coating method*

Below, we briefly compare the expected variation in thickness of the deposited liquid films using Taylor's method and our spin-coating method.

Imagine one wants to coat our tube with a 20 μm thick layer of 1000 cSt silicone oil. In Taylor's method, the oil is removed from one end of the tube with the syringe pump while the other end is exposed to air. When the oil completely wets the glass, the thickness of the film left behind follows Bretherton's scaling (Bretherton 1961),

$$h \sim R \left(\frac{\mu u}{\sigma}\right)^{2/3}. \tag{A 1}$$

One would need to draw out the silicone oil at $u = 0.36$ mm s^{-1} to leave a 20 μm film behind. Taking the variation of h with respect to u yields

$$\delta h \sim \frac{2R}{3} \left(\frac{\mu u}{\sigma}\right)^{2/3} \frac{\delta u}{u}. \tag{A 2}$$

The assumption of fully developed Poiseuille flow leads to $\delta u/u = \delta p/p$. If we take the characteristic value of normalized pressure fluctuations due to the syringe pump to be 1 % as in Zeng *et al.* (2015), then (A 2) gives an estimate of thickness variation to be $\delta h \sim 0.13$ μm.

Similarly, estimating the variation in thickness induced by fluctuation of angular velocity during spin coating, we use the results of figure 3(*c*), where the film thickness at sufficiently long time follows

$$h \sim \sqrt{\frac{3\mu}{2\rho\omega^2 t}}. \tag{A 3}$$

We would then need to spin 1000 cSt silicone oil for approximately 4 min to obtain a film thickness of 20 μm. Taking the variation of h with respect to ω:

$$\delta h \sim \sqrt{\frac{3\mu}{2\rho t}} \frac{\delta\omega}{\omega^2}. \tag{A 4}$$

The variation of thickness in the film for the angular velocity of 854 ± 10 r.p.m. yields $\delta h \sim 0.03$ μm, a variation about 4 times smaller than in Taylor's method.

REFERENCES

AUSSILLOUS, P. & QUÉRÉ, D. 2000 Quick deposition of a fluid on the wall of a tube. *Phys. Fluids* **12** (10), 2367–2371.

BICO, J. & QUÉRÉ, D. 2001 Falling slugs. *J. Colloid Interface Sci.* **243** (1), 262–264.

BLUNT, M. J. 2001 Flow in porous media pore-network models and multiphase flow. *Curr. Opin. Colloid Interface Sci.* **6** (3), 197–207.

BRETHERTON, F. P. 1961 The motion of long bubbles in tubes. *J. Fluid Mech.* **10** (02), 166–188.

CHENG, H. 2007 *Advanced Analytic Methods in Applied Mathematics, Science, and Engineering*. LuBan Press.

DUCLAUX, V., CLANET, C. & QUÉRÉ, D. 2006 The effects of gravity on the capillary instability in tubes. *J. Fluid Mech.* **556**, 217–226.

EGGERS, J. & VILLERMAUX, E. 2008 Physics of liquid jets. *Rep. Prog. Phys.* **71** (3), 036601.

EMSLIE, A. G., BONNER, F. T. & PECK, L. G. 1958 Flow of a viscous liquid on a rotating disk. *J. Appl. Phys.* **29** (5), 858–862.

DE GENNES, P.-G., BROCHARD-WYART, F. & QUÉRÉ, D. 2004 *Capillarity and Wetting Phenomena*. Springer Science & Business Media.

GOLDSMITH, H. L. & SPAIN, S. 1984 Margination of leukocytes in blood flow through small tubes. *Microvasc. Res.* **27** (2), 204–222.

GOREN, S. L. 1962 The instability of an annular thread of fluid. *J. Fluid Mech.* **12** (02), 309–319.

HOFFMAN, R. L. 1975 A study of the advancing interface. I. Interface shape in liquid–gas systems. *J. Colloid Interface Sci.* **50** (2), 228–241.

JOHNSON, M., KAMM, R. D., HO, L. W., SHAPIRO, A. & PEDLEY, T. J. 1991 The nonlinear growth of surface-tension-driven instabilities of a thin annular film. *J. Fluid Mech.* **233**, 141–156.

LI, Z., MAK, S. Y., SAURET, A. & SHUM, H. C. 2014 Syringe-pump-induced fluctuation in all-aqueous microfluidic system implications for flow rate accuracy. *Lab on a Chip* **14** (4), 744–749.

MORROW, N. R. & MASON, G. 2001 Recovery of oil by spontaneous imbibition. *Curr. Opin. Colloid Interface Sci.* **6** (4), 321–337.

MUGELE, F. & BARET, J.-C. 2005 Electrowetting: from basics to applications. *J. Phys.: Condens. Matter* **17** (28), R705–R774.

ODIER, C., LEVACHÉ, B., SANTANACH-CARRERAS, E. & BARTOLO, D. 2017 Forced imbibition in porous media: a fourfold scenario. *Phys. Rev. Lett.* **119** (20), 208005.

PATZEK, T. W. & KRISTENSEN, J. G. 2001 Shape factor correlations of hydraulic conductance in noncircular capillaries: II. Two-phase creeping flow. *J. Colloid Interface Sci.* **236** (2), 305–317.

PLATEAU, J. 1873 *Statique Expérimentale et Théorique des Liquides Soumis aux Seules Forces Moléculaires*. Gauthier-Villars.

PRIES, A. R., NEUHAUS, D. & GAEHTGENS, P. 1992 Blood viscosity in tube flow: dependence on diameter and hematocrit. *Am. J. Phys.* **263**, H1770–H1778.

RAYLEIGH, R. S. 1892 On the instability of cylindrical fluid surfaces. *Phil. Mag. J. Sci.* **34**, 177–180.

ROSSEN, W. R. 2000 Snap-off in constricted tubes and porous media. *Colloids Surf.* A **166** (1-3), 101–107.

SCRIVEN, L. E. 1988 Physics and applications of dip coating and spin coating. *MRS Proc.* **121**, 717–729.

TAYLOR, G. I. 1961 Deposition of a viscous fluid on the wall of a tube. *J. Fluid Mech.* **10** (02), 161–165.

WALLS, P. L. L., DEQUIDT, G. & BIRD, J. C. 2016 Capillary displacement of viscous liquids. *Langmuir* **32** (13), 3186–3190.

WASHBURN, E. W. 1921 The dynamics of capillary flow. *Phys. Rev.* **17** (3), 273–283.

ZENG, W., JACOBI, I., BECK, D. J., LI, S. & STONE, H. A. 2015 Characterization of syringe-pump-driven induced pressure fluctuations in elastic microchannels. *Lab on a Chip* **15** (4), 1110–1115.

ZHAO, B., ALIZADEH PAHLAVAN, A., CUETO-FELGUEROSO, L. & JUANES, R. 2018 Forced wetting transition and bubble pinch-off in a capillary tube. *Phys. Rev. Lett.* **120** (8), 084501.

ZHAO, B., MACMINN, C. W. & JUANES, R. 2016 Wettability control on multiphase flow in patterned microfluidics. *Proc. Natl Acad. Sci. USA* **113** (37), 10251–10256.